DIELECTRICS

High energy density in artificial heterostructures through relaxation time modulation

Sangmoon Han[1]†, Justin S. Kim[1,2]†, Eugene Park[3]†, Yuan Meng[1], Zhihao Xu[1,2], Alexandre C. Foucher[3], Gwan Yeong Jung[1,2], Ilpyo Roh[1,4], Sangho Lee[5], Sun Ok Kim[1,6], Ji-Yun Moon[1], Seung-Il Kim[1], Sanggeun Bae[1,2], Xinyuan Zhang[3], Bo-In Park[5], Seunghwan Seo[5,7], Yimeng Li[1], Heechang Shin[8], Kate Reidy[3], Anh Tuan Hoang[8], Suresh Sundaram[9], Phuong Vuong[9], Chansoo Kim[2,10], Junyi Zhao[2,10], Jinyeon Hwang[11], Chuan Wang[2,10], Hyungil Choi[4], Dong-Hwan Kim[6,12], Jimin Kwon[13], Jin-Hong Park[7], Abdallah Ougazzaden[9,14], Jae-Hyun Lee[15], Jong-Hyun Ahn[8], Jeehwan Kim[3,5], Rohan Mishra[1,2], Hyung-Seok Kim[11,16], Frances M. Ross[3]*, Sang-Hoon Bae[1,2]*

Electrostatic capacitors are foundational components of advanced electronics and high-power electrical systems owing to their ultrafast charging-discharging capability. Ferroelectric materials offer high maximum polarization, but high remnant polarization has hindered their effective deployment in energy storage applications. Previous methodologies have encountered problems because of the deteriorated crystallinity of the ferroelectric materials. We introduce an approach to control the relaxation time using two-dimensional (2D) materials while minimizing energy loss by using 2D/3D/2D heterostructures and preserving the crystallinity of ferroelectric 3D materials. Using this approach, we were able to achieve an energy density of 191.7 joules per cubic centimeter with an efficiency greater than 90%. This precise control over relaxation time holds promise for a wide array of applications and has the potential to accelerate the development of highly efficient energy storage systems.

Managing high energy density has become increasingly important in applications ranging from electric power systems to portable electronic devices (*1*–*3*). Electrostatic capacitors have been widely used for high energy storage and release owing to their ultrafast charge and discharge rate, but their performance is limited by the low maximum polarization (P_m) of conventional dielectric materials (*4*, *5*). By contrast, ferroelectric materials such as HfO_2, ZrO_2, and $BaTiO_3$ (BTO) can achieve higher maximum polarization because of their higher electric susceptibilities, which are related to dielectric constants (*6*, *7*). However, their high remnant polarization (P_r) limits the effectiveness of energy storage and release during the discharging process (*8*). To overcome this limitation, relaxor-ferroelectric materials have been studied for their ability to achieve high energy densities with low remnant polarization. Through compositional and defect design, nanodomains have been introduced into ferroelectric materials to realize relaxor ferroelectricity, offering a potential avenue for developing high-performance electrostatic capacitors (*9*, *10*). These methodologies lead to a redistribution of domain walls that can serve as effective relaxor-like defects to suppress the formation of large polar domains and reduce the remnant polarization. Although recent advances have shown great promise in realizing relaxor ferroelectricity by inducing nanodomains in ferroelectric materials through composition and defect engineering, these approaches result in the loss of crystallinity, which leads to reduced permittivity and sacrifices the maximum polarization. Moreover, some approaches are restricted from achieving a high polarization saturation limit, which results in polarization saturation at a low electric field and leads to low energy density (U_e), despite substantial breakthroughs otherwise (*11*). These limitations highlight the need for a different approach that can supplement previous methods and lead to the development of electrostatic capacitors with extremely high energy density.

We introduce a strategy for precise control of the relaxation time of polarization that maintains minimal energy loss by using monolayer two-dimensional (2D) materials produced by the layer-splitting technique (*12*). We achieved this by using artificially designed 2D/single-crystalline 3D/2D (2D/C-3D/2D) heterostructures. We used a layer-transfer technique to produce freestanding single-crystalline $BaTiO_3$ (C-BTO) in which both interfaces can be manipulated, and we formed 2D/C-3D/2D heterostructures by the addition of various 2D materials. Unlike previous approaches that deteriorate ferroelectric materials by involving structural changes, our approach preserves the single-crystal nature of the BTO. Instead, we sandwiched a C-BTO layer with 2D materials in the form of a freestanding membrane, such that the Maxwell-Wagner (MW) effect, a relaxation by charge accumulation at heterogeneous interfaces (*13*, *14*), takes place at the interfaces to change the relaxation time. Atomically precise control of the thickness of 2D materials by layer-resolved splitting (*15*, *16*) enables minimal energy loss and tangent delta (tan δ), a dielectric loss due to electrical phase difference (*12*, *17*), while controlling relaxation time. Using this strategy, we effectively suppressed the remnant polarization of ferroelectric materials while maintaining maximum polarization. We show that this allows for an energy density of 191.7 J/cm^3 with an efficiency greater than 90%. We believe our approach has the potential to enhance the performance of dielectric materials and be of use in other related applications that require high-energy storage systems.

MW relaxation at 2D/3D interfaces

The Miller model inspired by classic Debye relaxation provides a theoretical framework for controlling spontaneous polarization by manipulating the relaxation time (Fig. 1A). One approach for regulating the relaxation time involves the creation of heterostructures comprising two distinct materials, typically a ferroelectric material and a dielectric material, owing to their disparities in electrical conductivity and permittivity (*18*). These heterostructures enable the accumulation of charge at the interfaces between the phases when subjected to an alternating electric field, a phenomenon known as the MW relaxation effect. This effect offers a means to influence and modulate the relaxation time within the heterostructures. However, effective modulation of the relaxation time has been difficult to achieve while conserving maximum polarization in conventional heterostructures through the MW effect

[1]Department of Mechanical Engineering and Materials Science, Washington University in St. Louis, St. Louis, MO 63130, USA. [2]The Institute of Materials Science and Engineering, Washington University in St. Louis, St. Louis, MO 63130, USA. [3]Department of Materials Science and Engineering, Massachusetts Institute of Technology, Cambridge, MA 02139, USA. [4]M.O.P. Materials, Seoul 07285, Republic of Korea. [5]Department of Mechanical Engineering, Massachusetts Institute of Technology, Cambridge, MA 02139, USA. [6]Precision Biology Research Center, Sungkyunkwan University, Suwon 16419, Republic of Korea. [7]Department of Electrical and Computer Engineering, Sungkyunkwan University, Suwon 16419, Republic of Korea. [8]School of Electrical and Electronic Engineering, Yonsei University, Seoul 03722, Republic of Korea. [9]CNRS, Georgia Tech – CNRS IRL 2958, GT-Europe, 57070 Metz, France. [10]Department of Electrical and System Engineering, Washington University in St. Louis, St. Louis, MO 63130, USA. [11]Energy Storage Research Center, Korea Institute of Science and Technology, Seoul 02792, Republic of Korea. [12]School of Chemical Engineering, Sungkyunkwan University, Suwon 16419, Republic of Korea. [13]Department of Electrical Engineering, Ulsan National Institute of Science and Technology (UNIST), Ulsan 44919, Republic of Korea. [14]School of Electrical and Computer Engineering, Georgia Institute of Technology, Atlanta, GA 30332, USA. [15]Department of Materials Science and Engineering and Department of Energy Systems Research, Ajou University, Suwon 16499, Republic of Korea. [16]KHU-KIST Department of Converging Science and Technology, Kyung Hee University, Seoul 02447, Republic of Korea.

*Corresponding author. Email: fmross@mit.edu (F.M.R.); sbae22@wustl.edu (S.-H.B.)

†These authors contributed equally to this work.

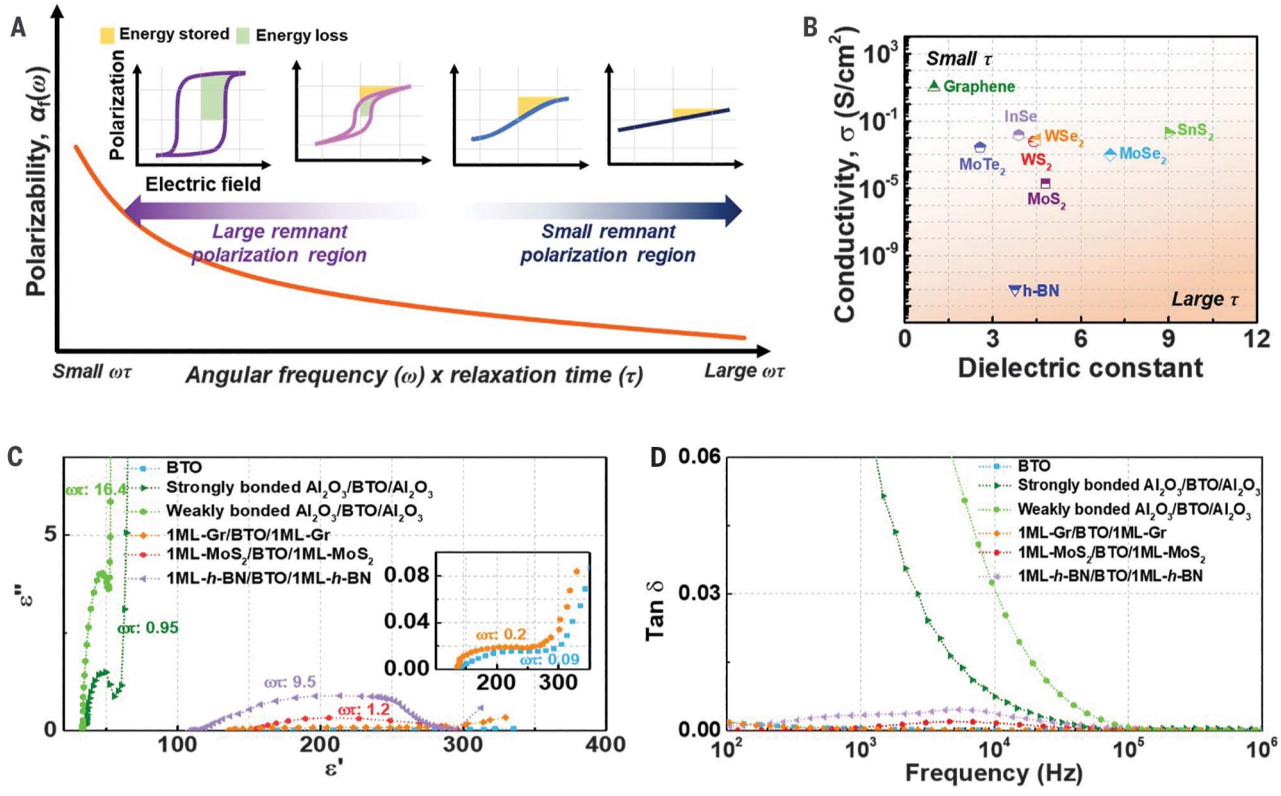

Fig. 1. Management of spontaneous polarization using the Miller model inspired from classic Debye relaxation. (**A**) Polarizability versus ωτ curve of the Miller model. (**B**) Summary of the conductivity versus dielectric constant curve of several 2D materials. (**C** and **D**) Dielectric Cole-Cole plots (C) and tan δ versus frequency curves (D) of the C-BTO, 2D/C-3D/2D, and 3D/C-3D/3D structures. ε′, real part of the dielectric constant; ε″, imaginary part of the dielectric constant.

for two reasons: (i) Previous attempts mainly led to the deterioration of ferroelectricity, generating strain or creating multidomain structures when the additional layers form chemical bonds with the ferroelectric material (*19*, *20*). (ii) As the thickness increases because of the additional layers that are needed for the MW effect, this inevitably leads to additional energy loss and a higher tan δ, which is closely associated with dielectric loss (*21*–*23*). We circumvented these problems by using 2D/C-3D/2D heterostructures formed using a layer-transfer technique (*24*–*26*). We first produced freestanding C-BTO with a thickness of 30 nm. The film is sufficiently high quality that we observed only the (001) orientation in electron back-scattering diffraction mapping. We used a variety of characterization techniques to show the C-BTO quality (figs. S1 to S4). A schematic representation of the 2D/C-BTO/2D fabrication process is shown in fig. S5. The freestanding nature of these C-BTO nanomembranes then allows us to coat both sides with other materials to produce artificial heterostructures.

We anticipated that choosing a 2D material for the coating layer would induce an efficient MW effect while avoiding substantial energy loss because of both the atomically thin nature of the 2D layers and the lack of strong chemical bonding at the heterointerfaces. To aid in 2D material choice, we summarize the conductivity versus dielectric constant of representative 2D materials in Fig. 2B (*27*–*33*). The higher the dielectric constant and the lower the conductivity, the stronger the MW relaxation induced at the interface. From the 2D candidates, we chose graphene (a 2D semimetal), MoS_2 (a 2D semiconductor), and hexagonal boron nitride (*h*-BN) (a 2D insulator). Although some studies of MoS_2 have shown ferroelectricity due to structural deformation, our previous measurements (*12*) of devices that included similar MoS_2 did not show such behavior, so we do not expect or include any ferroelectric behavior of the MoS_2 layer in our analysis. We selected these materials because we anticipated the possibility of observing diverse variations in relaxation time and tan δ within different artificial heterostructures. For comparison purposes, we also fabricated two different heterostructures of 3-nm-thick Al_2O_3/C-BTO/Al_2O_3. One heterostructure was formed by atomic layer deposition, for which we anticipated strong chemically bonded BTO/Al_2O_3 interfaces (fig. S6). We formed the other heterostructure by layer transfer without an annealing process and expected that it would lack strong chemically bonded interfaces (fig. S7).

After fabrication of this set of heterostructures, we measured the dielectric Cole-Cole plot at a frequency range of 10^2 to 10^6 Hz (Fig. 1C) and calculated the relaxation times at 10 kHz (fig. S8) (*34*, *35*). In the bare freestanding C-BTO nanomembranes, we obtained a value of ~0.09 for ωτ, which is defined as the product of angular frequency (ω) of 10 kHz and relaxation time (τ). We calculated the ωτ values of the Al_2O_3/C-BTO/Al_2O_3 samples to be 0.95 and 16.4 for the strongly and weakly bonded samples, respectively. We expect that some internal strain in the Al_2O_3 and C-BTO may be present, owing to the difference in thermal expansion coefficients, and any such effects are included in the relaxation times. This result indicates that the weakly bonded and discontinuous interface provides a higher relaxation time than that of a strongly chemically bonded interface (*36*, *37*). However, we measured the tan δ values of the strongly and weakly bonded Al_2O_3/C-BTO/Al_2O_3 to be 7.4×10^{-3} and 31.0×10^{-3} at 10 kHz, respectively, which are much higher than those of bare C-BTO (Fig. 1D). We expected substantial energy loss and a decrease in the maximum polarization density based on these values (*21*, *38*, *39*). By contrast, the heterostructures we fabricated using layer-resolved splitting of

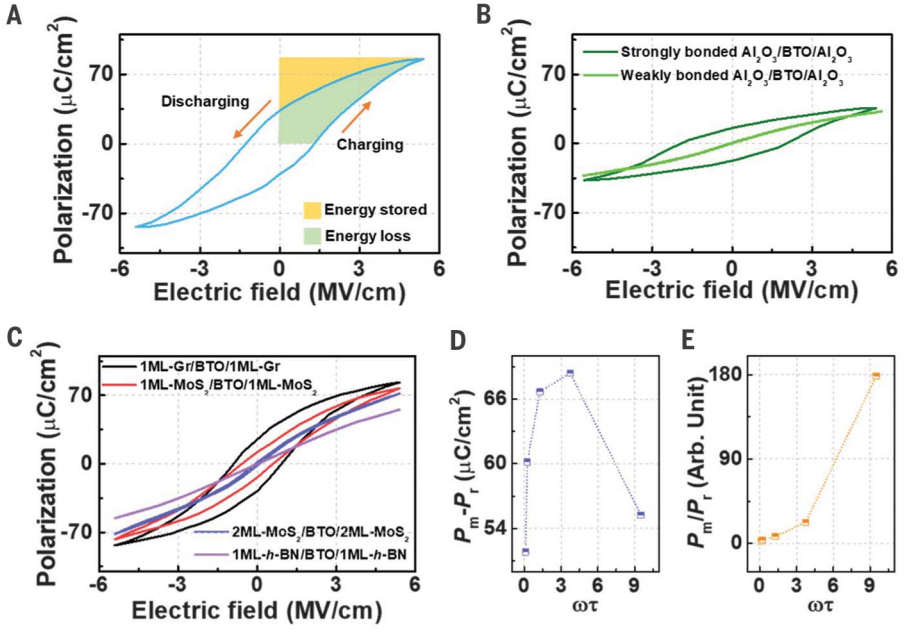

Fig. 2. Polarization of the C-BTO, 3D/3D/3D, and 2D/3D/2D heterostructures. (**A**) *P-E* loop of C-BTO. (**B**) Comparison of *P-E* loops of Al_2O_3/C-BTO/Al_2O_3 with strongly and weakly bonded interfaces. (**C**) *P-E* loop of the 2D/3D/2D heterostructure. The *P-E* loops were measured at 10 kHz. (**D** and **E**) $P_m - P_r$ (D) and P_m/P_r (E) calculated from the *P-E* loops.

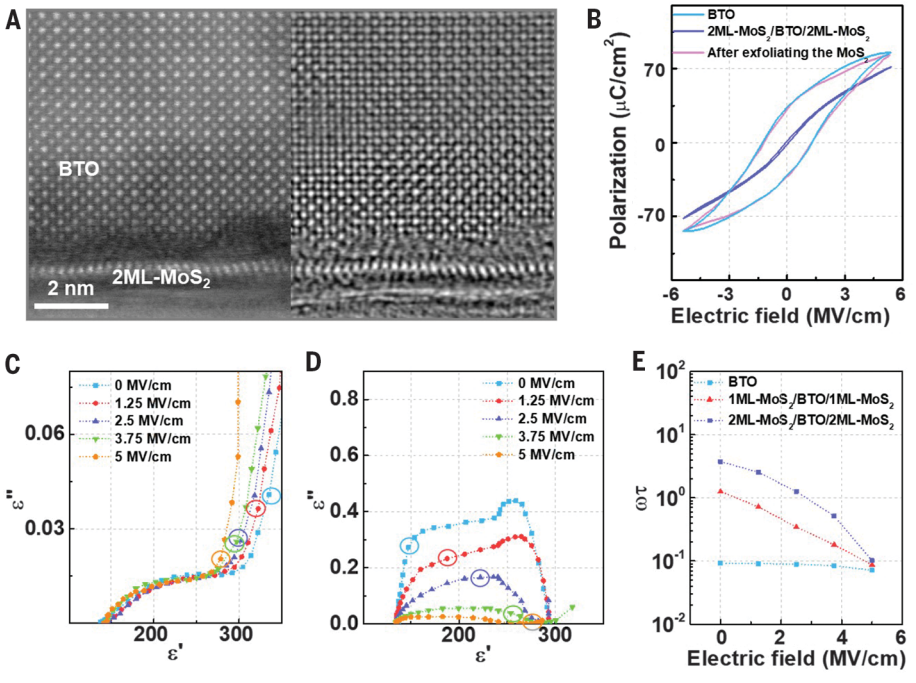

Fig. 3. Atomic-scale polarization distribution and additional electrical performance under bias. (**A**) STEM-HAADF (left) and iDPC (right) images of 2ML-MoS_2/C-BTO/2ML-MoS_2. Separation between the MoS_2 and BTO and interface roughness of the BTO are visible. (**B**) *P-E* loop of C-BTO, 2ML-MoS_2/C-BTO/2ML-MoS_2, and 2ML-MoS_2/C-BTO/2ML-MoS_2 after mechanically exfoliating the MoS_2 layers. (**C** and **D**) Dielectric Cole-Cole plots of C-BTO (C) and 2ML-MoS_2/C-BTO/2ML-MoS_2 (D) under dc bias electric field from 0 to 5 MV/cm. The circled values mean the ε′ and ε″ measured at 10 kHz. (**E**) The ωτ versus electric field of C-BTO, 1ML-MoS_2/C-BTO/1ML-MoS_2, and 2ML-MoS_2/C-BTO/2ML-MoS_2.

2D materials, which enabled thickness control of 2D materials at atomic precision (*15*, *26*), yielded lower tan δ and ωτ values. One–monolayer (ML) *h*-BN (1ML-*h*-BN)/C-BTO/1ML-*h*-BN had a ωτ of 9.5 and a tan δ of 3.7×10^{-3} at 10 kHz. More effective control of relaxation time is clearly achievable using *h*-BN compared with conventional dielectric materials such as Al_2O_3. Additionally, the lower tan δ with *h*-BN suggests the potential for relatively smaller energy loss using 2D materials. We attribute the benefits of the 2D material to its atomic thickness, compared with the relatively large Al_2O_3 layer thickness. To further explore our hypothesis, we repeated the experiment by creating an artificial heterostructure using MoS_2, which is known for its lower carrier density and dielectric constant, as well as graphene, which exhibits much lower values. The one-monolayer MoS_2 (1ML-MoS_2)/C-BTO/1ML-MoS_2 heterostructure had a ωτ value of 1.2 and a tan δ of 1.61×10^{-3}, whereas the one-monolayer graphene (1ML-Gr)/C-BTO/1ML-Gr heterostructure had a ωτ value of 0.2 and an even lower tan δ of 7.6×10^{-5}. Unlike the 1ML-*h*-BN/C-BTO/1ML-*h*-BN heterostructure, which displayed two distinct peaks, indicating the presence of MW relaxation (*40*, *41*), the 1ML-MoS_2/C-BTO/1ML-MoS_2 heterostructure did not exhibit clear peak separation, instead displaying an asymmetric Gaussian distribution. This still proves the presence of MW relaxation. However, the 1ML-Gr/C-BTO/1ML-Gr heterostructure did not show similar behavior in the tan δ measurement despite its extremely low tan δ. These findings highlight the role of the 2D materials in influencing and modulating relaxation time and tan δ within the heterostructures.

Polarization of artificial heterostructures

We expected that the large ωτ values that are caused by the large relaxation time would induce a strong reduction in the remnant polarization. We measured the polarization–electric field (*P-E*) loop of the unmodified C-BTO and the strongly and weakly chemically bonded Al_2O_3/C-BTO/Al_2O_3 heterostructures, all at 10 kHz (Fig. 2, A and B). Thirty-nanometer-thick BTO was chosen because it has a higher P_m, a lower P_r, and lower electrical leakage than other thicknesses that we tested (fig. S9). The maximum polarizations of both Al_2O_3/C-BTO/Al_2O_3 samples were substantially decreased because of the tan δ. However, the remnant polarization of the strongly bonded sample is much higher than that of the weakly bonded sample. These results agree with our expectation, driven by the tan δ and relaxation time values. Nevertheless, the Al_2O_3/C-BTO/Al_2O_3 with weakly bonded interfaces still provides low maximum polarization and thus poor energy storage performance because of the high tan δ attributed to the thick nature of Al_2O_3.

Based on our understanding that relaxation time can be controlled effectively while minimizing tan δ, we conducted *P-E* loop measurements on the various 2D/C-BTO/2D heterostructures (Fig. 2C). First, we examined *h*-BN/C-BTO/*h*-BN structures and observed a reduction in remnant polarization. However, this reduction also led to a decrease in maximum polarization, resulting in a notable decline in energy storage density and efficiency. To mitigate the decrease in maximum polarization, we used MoS_2, which possesses a higher conductivity than *h*-BN and is thus expected to minimize the MW relaxation. Indeed, when C-BTO was coated with 1ML-MoS_2, we observed a smaller decrease in maximum polarization. However, we also noted an insufficient decrease in remnant polarization, leading to energy loss. This insufficient decrease is attributed to the increase in conductivity of 1ML-MoS_2, for which we confirmed, through density functional theory calculations, the Fermi level shifts due to the metal contacts (fig. S10). Meanwhile, the successful suppression of the remnant polarization was observed in heterostructures using bilayer (2ML)-MoS_2, formed by sequentially transferring 1ML-MoS_2 twice, and C-BTO. We propose that the free electrons of the electrodes do not affect the MoS_2 layer adjacent to the C-BTO, which provides a sufficiently low conductivity to allow for screening of the dielectric polarization (fig. S11). We further investigated heterostructures containing graphene, which has a smaller dielectric constant. However, because of its high charge density, we were unable to induce an effective relaxation time delay. Instead, the *P-E* loop slightly decreased because of the small increase in the dielectric loss at the non–chemically bonded interface of the graphene/C-BTO (*42*). We attribute such performance, with small remnant polarization and high maximum polarization, to several factors: (i) The artificial heterostructures do not sacrifice the crystallinity of single-crystalline ferroelectric materials, unlike conventional heterostructures that experience lattice and thermal mismatch issues. (ii) The atomically thin 2D layers provide extremely low tan δ, preventing a high dielectric loss and decrease in the dielectric constant. (iii) The weakly bonded interface facilitates a substantial increase in dielectric relaxation even when the layer is atomically thin, effectively decreasing the remnant polarization. Together, we expect the small remnant polarization and large maximum polarization to lead to high energy density and high efficiency. To analyze which of the artificial heterostructures are most suitable for high energy density (Fig. 2, D and E), we subtracted the maximum polarization from the remnant polarization ($P_m - P_r$), which is related to the energy density, and divided the maximum polarization by the remnant polarization (P_m/P_r), which is related to the efficiency, according to the ωτ. Up to a ωτ value of 3.4, the $P_m - P_r$ and P_m/P_r values increased, indicating improved energy density and efficiency. For ωτ > 3.4, even though P_m/P_r increased, $P_m - P_r$ rapidly decreased. Considering these results, we therefore anticipated that the 2D/C-BTO/2D heterostructures with ωτ around 3.4 (1ML-MoS_2/C-BTO/1ML-MoS_2 and 2ML-MoS_2/C-BTO/2ML-MoS_2) provide the largest energy storage system in our samples (Cole-Cole plot of 2ML-MoS_2/C-BTO/2ML-MoS_2; fig. S12)

Atomic-scale polarization distribution

To gain a more comprehensive understanding of polarization behavior in the artificially designed 2D/C-3D/2D structures, we conducted

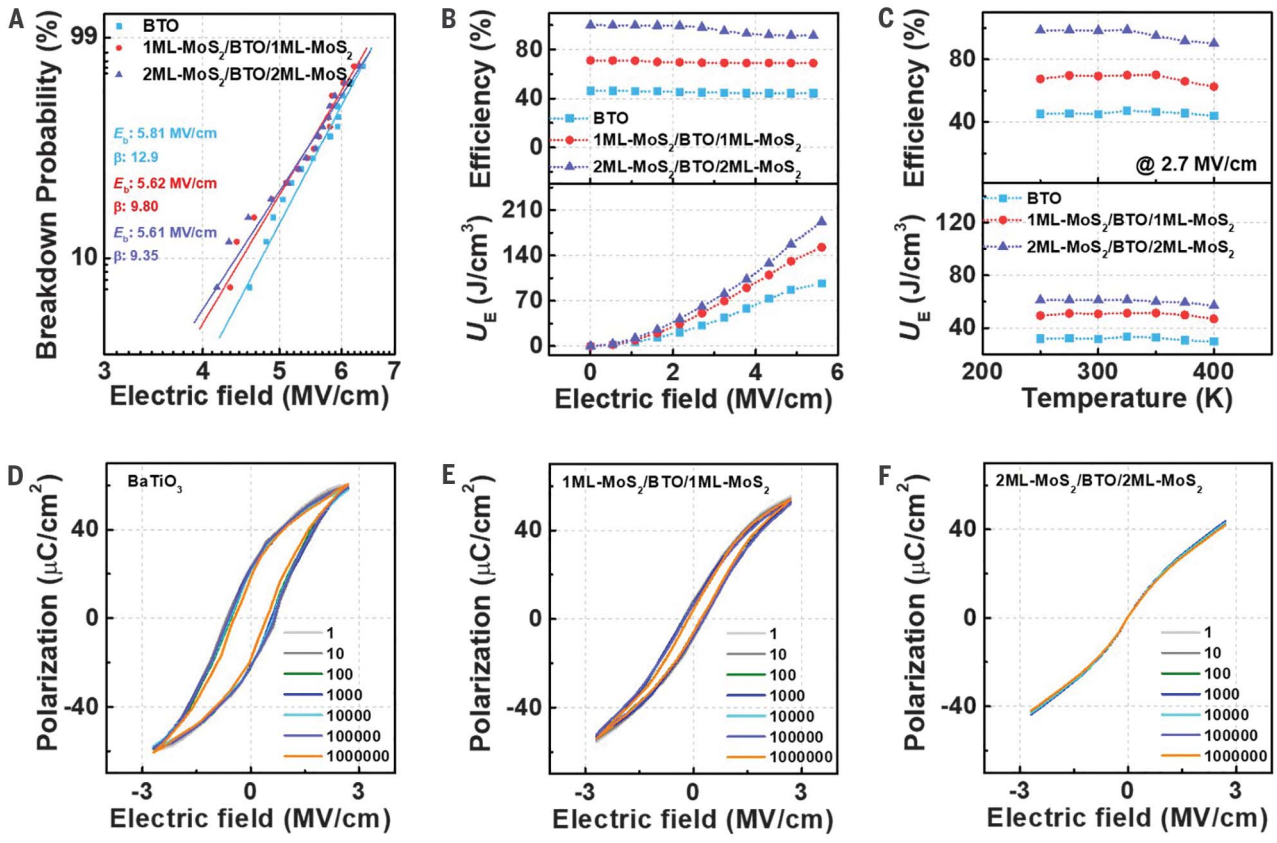

Fig. 4. Energy storage performance of C-BTO and MoS_2/C-BTO/MoS_2 with respect to the number of MoS_2 layers. (**A** and **B**) Two-parameter Weibull distribution analysis of the characteristic breakdown fields (A) and voltage-dependent energy density and efficiency of the C-BTO and MoS_2/C-BTO/MoS_2 heterostructures (B). (**C**) Temperature dependence of energy densities and efficiencies at temperatures ranging from 250 to 400 K. (**D** to **F**) *P-E* loops of C-BTO (D), 1ML-MoS_2/C-BTO/1ML-MoS_2 (E), and 2ML-MoS_2/C-BTO/2ML-MoS_2 (F) at temperatures ranging from 250 to 400 K.

additional electrical measurements and obtained atomic-scale structural information for the most effective structure, MoS_2/C-BTO/MoS_2. Figure 3A shows high-angle annular dark field (HAADF) and integrated differential phase contrast (iDPC) images of this sample measured by scanning transmission electron microscopy (STEM). We characterized the sample after hysteresis tests for 10 cycles under an electric field of −5 to 5 MV/cm at 10 kHz. We measured the lattice spacings of the C-BTO in all samples to be about 0.409 nm, corresponding to the (001) lattice plane of the BTO perovskite structure and indicating preferred growth along the [001] direction. Our HAADF and iDPC images clearly show the gap between the lattice structures of the 2ML-MoS_2 and C-BTO as well as some interfacial roughness (further example images are shown in fig. S13). Thus, structural discontinuity at the top and bottom surfaces of the C-BTO can work as a screener for dielectric polarization in the C-BTO crystal (*43*, *44*), leading to a relatively small remnant polarization. To further confirm the role of the 2D layer, we measured the *P-E* curve after mechanically exfoliating both the top and bottom MoS_2 layers from the 2ML-MoS_2/C-BTO/2ML-MoS_2 heterostructure. The hysteresis after removing the MoS_2 layers is similar to that of bare C-BTO (see the comparison in Fig. 3B), indicating that the pseudo-relaxor ferroelectric behavior exhibited by the 2D/3D/2D heterostructure is driven by charge compensation rather than relaxor ferroelectricity and that the 2D layers did not directly affect the dipoles inside the C-BTO crystal, preserving the high polarization.

Another intriguing aspect of our artificial 2D/3D/2D heterostructure is the observation that as the dc bias electric field increases, the polarization correspondingly increases, with the maximum polarization approaching that of C-BTO. This phenomenon indicates a strong correlation between the applied electric field and the relaxation time within the artificial heterostructure. We show the dielectric Cole-Cole plots of the C-BTO and 2ML-MoS_2/C-BTO/2ML-MoS_2 samples at a dc bias electric field of 0 to 5 MV/cm (Fig. 3, C and D), where the frequency-dependent dielectric constants are described in fig. S14. In the C-BTO sample, the $\omega\tau$ measured at 10 kHz is observed at the right side of the center of the semicircle regardless of the electric field. By contrast, the $\omega\tau$ of 2ML-MoS_2/C-BTO/2ML-MoS_2 measured at 10 kHz was shifted to the right with increased field, indicating an increase in the relaxation time. We summarize the $\omega\tau$ calculated from the dielectric Cole-Cole plot as a function of electric field for the C-BTO, 1ML-MoS_2/C-BTO/1ML-MoS_2, and 2ML-MoS_2/C-BTO/2ML-MoS_2 samples in Fig. 3E. The dc bias electric field-dependent Cole-Cole plot of MoS_2/C-BTO/MoS_2 is described in fig. S15. With increasing field, the relaxation times of the 2D/C-3D/2D become similar to those of the bare C-BTO. We attribute this result to the decrease in the accumulated charge by MW relaxation due to the electric field. This interplay between the electric field and relaxation time provides useful insights into the ferroelectric properties of the artificial 2D/3D/2D heterostructures.

Performance of MoS_2/C-BTO/MoS_2

To investigate the complete energy storage performance of the C-BTO and MoS_2/C-BTO/MoS_2 heterostructures, we measured their statistical breakdown strengths (E_b) by Weibull distribution fitting (Fig. 4A and fig. S16). We calculated the E_b values of the MoS_2/C-BTO/MoS_2 structures to be 5.62 and 5.61 MV/cm, which are comparable with that of C-BTO (5.81 MV/cm) owing to the low thickness of the C-BTO layer. Furthermore, our result is consistent with the negligible effective permittivity change arising from the atomically thin 2D layers (*1*). We observed nonzero leakage currents in the C-BTO and MoS_2/C-BTO/MoS_2 heterostructures (fig. S17), which are attributed to the narrow bandgap nature of BTO and the probability of oxygen vacancies (*45*, *46*). Nevertheless, the leakage current values are comparable to those of previously reported capacitors with high energy capability (*3*, *10*, *11*), indicating high reliability and E_b under high electric field conditions. From the *P-E* loops at 10 kHz, we further calculated the U_e and efficiencies of the samples at an electric field of ~5.6 MV/cm (close to their E_b) (Fig. 4B). As expected, we obtained a higher energy density from the 2ML-MoS_2/C-BTO/2ML-MoS_2 samples (191.7 J/cm^3) than from the C-BTO (96.9 J/cm^3) and 1ML-MoS_2/C-BTO/1ML-MoS_2 (152.4 J/cm^3) samples. The energy density we observed in the 2ML-MoS_2/C-BTO/2ML-MoS_2 heterostructure exhibits a high value (fig. S18). These ultrahigh U_e values are the combined results of high polarization density, low hysteresis, and high efficiency (greater than 90%). The high efficiency is critical to address the energy dissipation of dielectrics for high-power applications, facilitating reliable operation. At higher frequency, smaller P_m and P_r were observed because there is insufficient time to align the dipoles at the higher frequency (fig. S19). Nevertheless, high energy storage performance is still achieved. We also conducted stability and reliability tests, which are crucial for electrostatic energy storage. For a thermal stability test, we measured the *P-E* loops of the MoS_2/C-BTO/MoS_2 structures, which showed good stability of the polarization (fig. S20) and energy storage performance (Fig. 4C) under a wide temperature range (250 to 400 K) with a small degradation in U_e (<6%) and efficiency (<6%). We attribute this U_e and efficiency reduction to the complex thermal scattering of charges accumulated at the non–chemically bonded interfaces (*47*). Nevertheless, the degradation rates are similar to previously reported results, indicating good thermal stability (*9*, *48*, *49*). They survived over 10^8 cycles during an accelerated charge-and-discharge test, as shown in Fig. 4, D to F. Moreover, the degradation rate of 2ML-MoS_2/C-BTO/2ML-MoS_2 is <5% after 10^8 cycles, indicating that our samples are stable during the cycling test. To assess the practical feasibility of our approach, we fabricated a 2ML-MoS_2/C-BTO/2ML-MoS_2 array (fig. S21). The average P_m is 36.3 ± 9.3 μC/cm^2 at 2.7 MV/cm with suppressed P_r, indicating the potential for practical application.

Conclusions

Our findings highlight the complex interplay between different materials in artificially designed 2D/C-3D/2D heterostructures and their impact on remnant polarization, maximum polarization, energy loss, and efficiency. These insights contribute to the understanding of how to optimize the design and performance of high-energy electrostatic capacitors using ferroelectric materials. By using this approach, we anticipate that future advances can be achieved in the development of more efficient and giant energy storage systems.

REFERENCES AND NOTES

1. J.-K. Huang *et al.*, *Nature* **605**, 262–267 (2022).
2. A. J. Yang *et al.*, *Nat. Electron.* **5**, 233–240 (2022).
3. H. Pan *et al.*, *Science* **374**, 100–104 (2021).
4. Q. Li *et al.*, *Nature* **523**, 576–579 (2015).
5. H. Luo *et al.*, *Adv. Sci.* **9**, e2202438 (2022).
6. X.-K. Wei *et al.*, *Adv. Mater.* **32**, e2003479 (2020).
7. J. P. B. Silva, K. C. Sekhar, H. Pan, J. L. MacManus-Driscoll, M. Pereira, *ACS Energy Lett.* **6**, 2208–2217 (2021).
8. L. Yang *et al.*, *Prog. Mater. Sci.* **102**, 72–108 (2019).
9. T. Li *et al.*, *Adv. Funct. Mater.* **32**, 2202307 (2022).
10. B. Yang *et al.*, *Nat. Mater.* **21**, 1074–1080 (2022).
11. J. Kim *et al.*, *Science* **369**, 81–84 (2020).
12. J. Shim *et al.*, *Science* **362**, 665–670 (2018).
13. Z. Wu *et al.*, *Adv. Mater.* **34**, e2107538 (2022).
14. M. Qin, L. Zhang, H. Wu, *Adv. Sci.* **9**, e2105553 (2022).
15. S.-H. Bae *et al.*, *Proc. Natl. Acad. Sci. U.S.A.* **114**, 4082–4086 (2017).
16. M. T. Sebastian, R. Ubic, H. Jantunen, *Int. Mater. Rev.* **60**, 392–412 (2015).
17. T. Rahman, M. Vargas, R. Chintalapalle, *J. Alloys Compd.* **617**, 547–562 (2014).
18. S. S. Cheema *et al.*, *Nature* **604**, 65–71 (2022).
19. H. W. Park *et al.*, *Adv. Funct. Mater.* **33**, 2206637 (2023).
20. Y. J. Kim *et al.*, *Sci. Rep.* **6**, 19039 (2016).
21. A. K. Saha, M. Si, P. D. Ye, S. K. Gupta, *Appl. Phys. Lett.* **119**, 122903 (2021).
22. J. P. B. Silva *et al.*, *J. Mater. Chem. A Mater. Energy Sustain.* **8**, 14171–14177 (2020).
23. Z. Wu *et al.*, *ACS Appl. Mater. Interfaces* **10**, 11108–11115 (2018).
24. J. Shin *et al.*, *Nature* **614**, 81–87 (2023).
25. H. Kim *et al.*, *Nat. Nanotechnol.* **18**, 464–470 (2023).
26. S.-H. Bae *et al.*, *Nat. Mater.* **18**, 550–560 (2019).
27. A. Laturia, W. G. Vandenberghe, in *2017 International Conference on Simulation of Semiconductor Processes and Devices (SISPAD)* (IEEE, 2017), pp. 337–340.
28. H. Zhou, Y. Cai, G. Zhang, Y.-W. Zhang, *Nanoscale* **10**, 480–487 (2017).
29. J.-H. Ahn *et al.*, *Nano Lett.* **15**, 3703–3708 (2015).
30. S.-I. Kim *et al.*, *Synth. Met.* **299**, 117464 (2023).
31. A. Perepeliuc *et al.*, *Appl. Phys. Lett.* **122**, 263503 (2023).
32. S. Hwangbo, L. Hu, A. T. Hoang, J. Y. Choi, J.-H. Ahn, *Nat. Nanotechnol.* **17**, 500–506 (2022).
33. Y. Ahn, M. Shin, *IEEE Trans. Electron Dev.* **64**, 2129–2134 (2017).

34. T. A. Hanafy, K. Elbanna, S. El-Sayed, A. Hassen, *J. Appl. Polym. Sci.* **121**, 3306–3313 (2011).
35. H. Wang, L. Yang, X. Zhang, M. H. Ang Jr., *Results Phys.* **29**, 104781 (2021).
36. B.-H. Fan *et al*., *Compos. Sci. Technol.* **80**, 66–72 (2013).
37. K. Venkateshan, G. P. Johari, *J. Chem. Phys.* **125**, 014907 (2006).
38. M. H. Park, H. J. Kim, Y. J. Kim, T. Moon, C. S. Hwang, *Appl. Phys. Lett.* **104**, 072901 (2014).
39. M. Liu *et al*., *ACS Appl. Mater. Interfaces* **4**, 5761–5765 (2012).
40. M. Samet *et al*., *J. Chem. Phys.* **142**, 194703 (2015).
41. H. Hammami, M. Arous, M. Lagache, A. Kallel, *J. Alloys Compd.* **430**, 1–8 (2007).
42. Y. G. Lee *et al*., *Appl. Phys. Lett.* **98**, 183508 (2011).
43. T. Akamatsu *et al*., *Science* **372**, 68–72 (2021).
44. Y. Liu, Y. Huang, X. Duan, *Nature* **567**, 323–333 (2019).
45. S. H. Kim *et al*., *Phys. Status Solidi Rapid Res. Lett.* **13**, 1900373 (2019).
46. M. Pawlak *et al*., *Appl. Phys. Lett.* **101**, 042901 (2012).
47. J. Yang *et al*., *Nat. Nanotechnol.* **7**, 91–95 (2012).
48. H. Qi *et al*., *Adv. Funct. Mater.* **29**, 1903877 (2019).
49. D. Li *et al*., *Small* **19**, e2206958 (2023).

ACKNOWLEDGMENTS

Funding: S.-H.B. acknowledges support from the Institute of Materials Science and Engineering (IMSE), Washington University in St. Louis. S.-H.B. acknowledges financial support from the National Science Foundation (grant no. 2240995). S.-H.B. also acknowledges that this work was partially supported by Samsung Electronics Co., Ltd. (IO221219-04250-01). D.-H.K. acknowledges support from a Korea Institute for Advancement of Technology (KIAT) grant funded by the Korean government (MOTIE) [P0017305, Human Resource Development Program for Industrial Innovation (Global)]. J.-H.A. was supported by the National Research Foundation of Korea (2015R1A3A2066337). A.O. acknowledges financial support from Georgia Tech Europe in Metz-France. R.M. was supported by the Army Research Office (ARO) Multidisciplinary University Research Initiative (MURI) under award no.W911NF-21-1-0327 and the NSF through DMR-2122070 and DMR-2145797. This work used computational resources through allocation DMR160007 from the Advanced Cyberinfrastructure Coordination Ecosystem: Services & Support (ACCESS) program, which is supported by the NSF. This work was carried out in part through the use of MIT.nano's facilities. E.P. acknowledges funding from a MathWorks fellowship. **Author contributions:** S.-H.B., S.H., and J.S.K. conceived this study. J.S.K., E.P., Y.M., Z.X., I.R., S.O.K., and Y.L. fabricated the samples and performed the experiment, with the supervision of S.-H.B. and S.H. S.L., X.Z., and B.-I.P. performed the structural performance of samples, under the supervision of J.Ki. J.-Y.M., S.-I.K., H.S., A.T.H., S.Su., P.V., A.O., J.-H.L., and J.-H.A. prepared the 2D materials. G.Y.J. reviewed the theory about dielectric relaxation under the supervision of R.M. E.P., A.C.F., and K.R. performed the STEM and iDPC characterization under the supervision of F.M.R. S.Se. and J.-H.P. analyzed the 2D/3D and 3D/3D interfaces. S.B., C.K., J.Z., C.W., J.Kw., and D.-H.K. performed the electrical measurement. J.H., H.C., and H.-S.K. conducted the breakdown performance. S.-H.B. and S.H. wrote the first draft of the manuscript. All authors discussed the results and revised the manuscript. **Competing interests:** S.H. and S.-H.B. are inventors on patent application no. 63/617,314 assigned to Washington University that covers heterostructures that have a van der Waals interface for high–energy density capacitors. **Data and materials availability:** All data are available in the main text or the supplementary materials.

SUPPLEMENTARY MATERIALS

science.org/doi/10.1126/science.adl2835
Materials and Methods
Supplementary Text
Figs. S1 to S21
References (*50*–*76*)

Submitted 10 October 2023; accepted 6 March 2024
10.1126/science.adl2835